

Convolutional Neural Network for Battery System Monitoring and SOC Estimation for Ev Applications to Achieve Sustainability

Priya. S^{1,*}, Vinoth Kumar. P², Sridevi. V³, M. Batumalay⁴, Gunapriya D⁵

^{1,3}AMET Deemed to be University, Kanathur, Chennai 603112, Tamil Nadu,

²India Department of Electrical and Electronics Engineering, Sri Krishna College of Engineering and Technology, Tamil Nadu, India

⁴Faculty of Data Science and Information Technology, INTI International University, 71800 Nilai, Malaysia

Department of Electrical and Electronics Engineering, Sri Eshwar College of Engineering, Coimbatore, Tamil Nadu, India

(Received: August 24, 2024; Revised: September 14, 2024; Accepted: September 24, 2024; Available online: October 20, 2024)

Abstract

The necessity to develop an alternative energy source to handle the looming energy crisis has arisen due to the recent rise in energy consumption. This is most likely to happen with grid-synchronized electric vehicles (EVs), since vehicle-to-grid (V2G) technology is one of the smart grid's technological advancements that permits energy exchange between EVs and the grid. The merging of EVs with the grid influences the whole electricity system and is susceptible to imbalances in supply and demand, frequency, and voltage. The proposed work focuses on effective and smart control of the Single Ended Primary Inductance Converter (SEPIC) converter with efficient control techniques employed for battery management systems for electric vehicle charging. PI oversees controlling the converter. The battery's calculated state of charge (SOC) is used to make a paradigm-shifting sequence for the converter with workable optimization strategies to lower imbalance issues when EVs are connected to the grid. This leads to the achievement of sustainable development goals (SDGs). Purpose. When the SEPIC converter is connected to a photovoltaic source, it needs to be analyzed in terms of how it switches operations. The source also needs to be used efficiently when it is connected to a battery. Monitoring and SOC estimation of the battery need to be efficiently performed with a quicker response for EV applications. Methods. Convolutional neural networks (CNN) were used to solve the issue; these networks considerably enhance response times and boost system reliability overall. Results. The system operates on the principle that when the battery level is less than 60%, the battery is charged through buck operation, and it is discharged through the boost mode when the SOC exceeds 60%. When linked to the grid, the PI controller regulates both power and practical value. The proposed system demonstrates how battery management-based CNN and SEPIC can switch at high speeds. The system's research directions were established for the results' later application to experimental samples for energy efficiency and process innovation.

Keywords: Electric Vehicle, State Of Charge, Convolutional Neural Network, SEPIC Converter, Sustainable Development Goals (SDG), Energy Efficiency, Process Innovation

1. Introduction

Electric vehicles (EVs) have gained significant traction in recent years due to their substantial contribution to reducing greenhouse gas emissions, making them a crucial solution in mitigating climate change. However, numerous challenges persist in ensuring the efficient operation of EVs. These challenges primarily revolve around the complex control of motor drives, power management in controllers, battery energy management, and optimization of input resources [1]. Addressing these challenges is essential to enhance the overall performance and efficiency of EVs.

As the functionality of EVs expands and battery utilization efficiency decreases during operation, the need for fast charging and quick response times becomes more critical. Power electronics converters play a pivotal role in managing grid interfaces and providing galvanic isolation, which are essential for both motor operation and battery charging in EVs [2]. The battery charging infrastructure, whether grid-connected or standalone, is another vital component in the EV ecosystem [3]. When connecting EVs to the grid, factors such as voltage stability and transformer capacity must

*Corresponding author: Priya. S (priasakthikumar@gmail.com)

DOI: <https://doi.org/10.47738/jads.v5i4.237>

This is an open access article under the CC-BY license (<https://creativecommons.org/licenses/by/4.0/>).

© Authors retain all copyrights

be carefully considered [4]. The growing adoption of electric vehicles has also spurred the increased use of renewable energy sources, particularly photovoltaic (PV) systems, for home charging solutions. Optimizing energy use and improving battery performance, based on parameters such as temperature, electricity consumption, and charging rates, are critical factors to consider [5]. Smart batteries equipped with integrated battery management systems (BMS) and DC-DC converters are essential for efficient control of both charging and discharging processes. These converters not only enhance system resilience but also facilitate maximum power point tracking (MPPT) and adaptive charging in response to load fluctuations [6], [7].

This study aims to design a non-isolated SEPIC converter with integrated battery management capabilities, such as battery charge management, and to demonstrate the practical application of this concept in real-world scenarios. The control signal is generated by a convolutional neural network (CNN) controller, while pulse-width modulation (PWM) pulses regulate the switching actions of the SEPIC converter, ensuring controlled operation without distortion. This approach is particularly suitable for controlled DC operations, such as charging EV batteries.

2. Literature Review

Bin Liu et al. [8] emphasize the importance of proper control of photovoltaic (PV) inverters when converting solar energy systems to home panels or battery systems. Effective control helps reduce input current ripple and grid-current harmonics. Their findings suggest that the low internal impedance of batteries is insufficient to dampen the ripple current caused by the grid-connected inverter, presenting a fundamental challenge [9]. To address this, an innovative active control mechanism based on the fragile signal model of a DC-DC converter is introduced. This approach utilizes a dual-channel current feedback system—one for the main channel and another for ripple current feedback. A third-order general integrator is implemented to extract the ripple current and transmit the feedback signal.

In the context of electric vehicle (EV) charging infrastructure, the development of DC fast charging station (CS) networks has been a focal point, with efforts to reduce implementation costs while maintaining high-quality charging experiences, such as minimizing wait times and reducing charging distances. These networks maintain a steady flow of electricity by deploying a minimal number of power modulators and using rated transformers to manage peak demand, while also accounting for the limitations of the energy distribution grid.

Mostafa M. Mahfouz et al. [10] evaluated a system design and control architecture that mitigates the impact of EV DC fast charging stations on their host AC grids, which are often under strain. Their study highlights a control system that decouples the charging station dynamics from the grid and incorporates a battery energy retention system to ensure stability during rapid charging.

Nupur Saxena et al. [11] proposed that power and load leveling can be achieved by controlling the battery's charging and discharging cycles, which also improves system reliability. The multifunctional voltage-source converter in their system serves multiple roles, including reactive power correction, harmonic mitigation, and acting as an active power filter. A novel control system is employed to resynchronize the electrical network after fault mitigation and upon reconnection. In a related study, Rahmat Khezri et al. [12] explored the optimal sizing of solar photovoltaic (PV) and buffer energy storage capacity for grid-tied homes, aiming to minimize the real-time cost of electricity. Their optimization process used real-time domestic energy monitoring systems that considered annual solar radiation data, ambient temperature, household energy consumption, and energy prices [9]. Two system configurations were evaluated: one with solar PV and the other with battery energy storage (BES).

Vishnu Mahadeva Iyer et al. [13] introduced a strategy for the electrical execution of an ultra-fast charging (XFC) station designed to charge multiple EVs simultaneously [1]. By employing DC-DC converters for fractional energy handling, the proposed method eliminates the need for redundant energy conversions. This approach allows individual control of each EV's charging process, handling only a portion of the total power required for battery charging. However, the system still exhibits limitations in terms of accuracy due to energy-wasting oscillations in steady-state conditions. Reducing the perturbation step size can minimize these oscillations, but at the cost of slower maximum power point (MPP) tracking. Furthermore, these systems face challenges in rapidly changing environmental conditions.

The current study introduces a State of Charge (SOC) prediction framework for battery energy storage systems (BESS) utilizing a CNN strategy. The integration of a CNN-assisted SEPIC converter can enhance and stabilize the low DC output voltage provided by PV systems. CNN, as a feedforward neural network, effectively manages the charging and discharging processes of batteries with accurate SOC estimation. Given the fluctuating nature of photovoltaic energy sources, energy storage systems like batteries are critical for maintaining reliable power supply and energy balance. The SOC is used to regulate the battery's charging and discharging processes with the aid of the CNN controller.

3. Smart Battery Monitoring system and linkage with SDG

SOC estimation for electric vehicle (EV) applications plays a crucial role in advancing several Sustainable Development Goals (SDGs) by fostering innovation, improving energy efficiency, supporting sustainable community development, and contributing to global warming mitigation efforts. Convolutional neural networks (CNNs) are particularly promising in SOC estimation and battery system monitoring, as they enhance the performance and longevity of EV battery management systems, ultimately promoting the adoption of renewable energy technologies. Through optimized battery management, CNNs can increase energy efficiency and extend battery life, thereby supporting the transition to cleaner energy sources. Implementing sophisticated monitoring systems, such as CNNs, improves the infrastructure necessary for sustainable industries and drives innovation in renewable energy technologies [14]. This aligns SOC estimation with SDG 9: Industry, Innovation, and Infrastructure, as well as SDG 7: Affordable and Clean Energy.

A SEPIC converter controlled by a proportional-integral (PI) controller can efficiently manage the power supply in systems utilizing renewable energy sources, such as solar and wind generation. By enhancing the efficiency of energy conversion and storage, PI-controlled SEPIC converters facilitate the shift towards renewable energy sources, making clean and affordable energy more accessible. The use of advanced control techniques, such as PI control in power converters, promotes innovation in renewable energy and power electronics, further supporting the development of sustainable infrastructure for the green energy sector [15].

The development of sustainable cities and communities is closely linked to the implementation of renewable energy systems and electric vehicles. Efficient power conversion systems, regulated by PI controllers, play a critical role in reducing air pollution and enhancing energy resilience in urban areas. Furthermore, CNN-based monitoring systems for EV batteries contribute to more efficient and reliable energy storage, aiding in the development of sustainable urban transport systems [16]. This supports SDG 11: Sustainable Cities and Communities by reducing emissions and the negative environmental impacts of transportation. Additionally, the optimization of battery usage and accurate SOC calculation ensure optimal charging and discharging cycles, minimizing energy consumption and mitigating adverse ecological effects, which aligns with SDG 13: Climate Action. The successful deployment of advanced power conversion systems requires collaboration among technology developers, energy providers, policymakers, and other stakeholders. By fostering knowledge exchange, resource mobilization, and capacity building, these collaborations accelerate progress toward achieving sustainable development goals [17], [18]. In this context, the proposed work leverages SOC monitoring systems and battery management to contribute to the realization of these goals.

3.1. Proposed Converter Analysis

The VLV and VHV, respectively, indicate the low voltage and high voltage sides. Two inductors, L1 and L2, four capacitors, C1, C2, and Co (1, 2), and five switches, S1, S2, Q1, Q2, and Q3, make up the suggested dc-dc converter. Throughout the whole switching period (T_s), the switches and body diodes operate in parallel. As also shown in figure 1, to connect the bidirectional DC-DC converter to the AC grid, a conventional single-phase full-bridge DC-AC converter with unipolar PWM modulation is used. The DC-AC converter's four switches—SA, SB, SC, and SD—operate conventionally in terms of fundamental PWM operation. On the grid side of the DC-AC, Lg is the moniker of an inductive filter [19], [20]. The dc-dc converter's step-down and step-up modalities are depicted in figure 2 and figure 3, along with the continuous conduction mode (CCM) and discontinuous conduction mode (DCM). A comprehensive review of each mode is provided below.

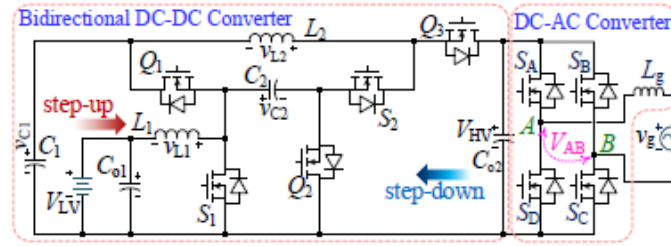


Figure 1. Proposed Bidirectional converter circuit

3.2. Step Down Mode

The proposed converter operates in step-down mode, as illustrated in figure 2, which shows the corresponding circuit in different operational stages. In the first state of Continuous Conduction Mode (CCM), from time 0 to t_1 , the high-voltage (VHV) side is connected to a DC supply, while the low-voltage (VLV) side is connected to the load. During this period, switches Q1, Q2, and Q3 are turned on, while S1 and S2 remain off, as shown in figure 2(a). Energy is supplied from capacitor C1 and the incoming DC source to charge inductor L2. At the same time, the energy stored in L1 is increased by the charge from capacitor C2, causing the current through L2 to rise.

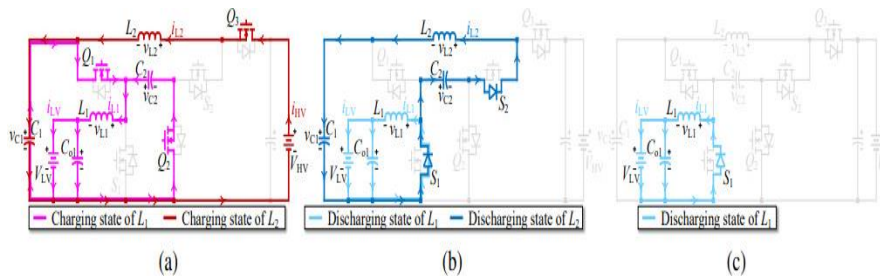


Figure 2. The suggested converter's corresponding circuit in step-down mode: Positions 1 through 3 are (a), (b), and (c).

In the second state, spanning from time t_1 to T_s , the operation shifts between Continuous Conduction Mode and Discontinuous Conduction Mode (DCM). During this period, switches Q1, Q2, and Q3 are turned off, and the body diodes of S1 and S2 begin to conduct, as shown in figure 2(b). Energy stored in inductor L2 is released into capacitors C1 and C2. Additionally, the energy stored in inductor L1 is transferred to the VLV side, supporting the load during this phase.

The third state occurs in the Discontinuous Conduction Mode (DCM) between time t_2 and t_3 , near the end of the switching period, as shown in figure 2(c). At time t_2 , the current in inductor L2 reaches zero, and similarly, at time t_3 , the current in inductor L1 also falls to zero. This marks the transition to the final state of the step-down mode.

In the fourth and final state of the step-down mode, occurring between time t_3 and T_s , all power switches are turned off. As a result, the current in the circuit through the inductors drops to zero, completing the energy transfer cycle and bringing the converter to rest before the next switching period begins.

3.3. Step Up Mode

The converter also operates in step-up mode, as depicted in figure 3, with the circuit going through several distinct operational states. In the first state of Continuous Conduction Mode (CCM), from time 0 to t_1 , energy is transferred from the low-voltage (VLV) side to the high-voltage (VHV) side. As shown in figure 3(a), switches S1 and S2 are turned on, while Q1, Q2, and Q3 are turned off. During this phase, the input DC source charges inductor L1. Simultaneously, capacitors C1 and C2 increase the energy in L2, causing the current through L2 to rise.

In the second state, between time t_1 and T_s , the operation alternates between Continuous Conduction Mode and Discontinuous Conduction Mode (DCM). In this phase, switches S1 and S2 are turned off, and the body diodes of Q1, Q2, and Q3 conduct, as shown in figure 3(b). Energy from inductor L2 is released into capacitors C1 and C2, while the energy stored in inductor L1 is transferred to the VLV side, supplying power to the load.

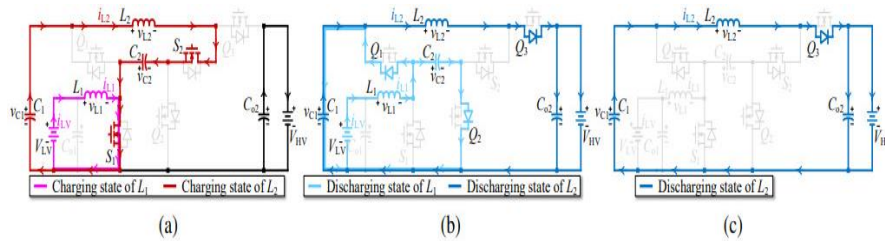


Figure 3. shows the suggested converter's corresponding circuit operating in step-up mode. Positions 1 through 3 are (a), (b), and (c).

The third state, occurring in Discontinuous Conduction Mode (DCM) from time t_2 to t_3 , takes place just before the end of the switching period, as illustrated in [figure 3\(c\)](#). During this phase, the current in inductor L_2 reaches zero at time t_2 , followed by the current in inductor L_1 reaching zero at time t_3 . This marks the near-completion of the energy transfer process. In the fourth and final state, from time t_3 to T_s , all power switches are off. At this point, the current through the inductors drops to zero, concluding the switching cycle. The converter is then ready for the next operation, having successfully transferred energy from the VLV side to the VHV side.

3.4. Control System

The control of the proposed converter consists of the LV side (or battery current) voltage control during a constant voltage (CV) loop and the LV side (or battery current) current control during a constant current (CC) loop. [Figure 4](#) displays the suggested control system's overall diagram. This converter uses a straightforward, quick, and effective digital dead-beat current control technique in both directions. Typically, the full-charge voltage of the battery is designated as the LV side voltage reference, V^*_{LV} (or V^*_{bat}). The current reference is on the LV side. When the battery is not completely charged, I^*_{LV} (or I^*_{bat}) is seen.

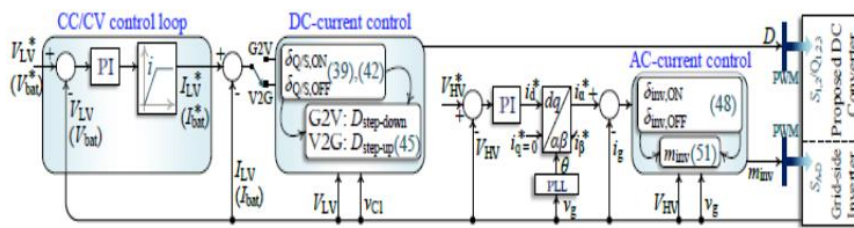


Figure 4. The overall control system of proposed EV charger

The limiter in the CC/CV mechanism causes the output of the PI compensator to become saturated when the battery is not fully charged, and the limiter's upper limit value determines the battery current reference. The compensation for PI triggers the voltage governor hoop to manage the voltage of the battery when VLV reaches the full-charge voltage. Two control loops are used: an exterior PI-based dc voltage control loop and an inside current control loop based on dead-beat control to govern the dc side voltage, or VHV, of the inverter employed as a grid interface. The PI compensator and limiter's outputs serve as the dead-beat current control loop's reference points. With the measured and reference current through L_1 and the VLV and C_1 voltages, the proposed dead-beat current controller can easily figure out the right duty cycle for both the step-down and step-up modes.

3.5. SEPIC Converter Operation

The SEPIC (Single-Ended Primary Inductor Converter) is a versatile DC-DC converter that effectively converts the variable output from solar panels into a stable voltage suitable for powering loads or charging batteries, which is critical in solar power systems where optimizing energy harvest is essential. As illustrated in [figure 5](#), the SEPIC converter can produce an output voltage that is either higher, lower, or equal to the input voltage, depending on the operating conditions. The circuit includes an active power switch, MOSFET (T), to control the switching operations, as well as other key components such as a diode (D), two inductors (L_A and L_B), and two capacitors (C_c and C_O) [12].

When the MOSFET (T) is turned on, as shown in [figure 6](#), inductors LA and LB are charged by the input voltage (Vi) and the voltage across capacitor Cc. The diode D operates in reverse-biased mode due to the negative polarity of the coupling capacitor Cc. During this period, both inductors accumulate energy as the coupling capacitor discharges.

When the MOSFET (T) is turned off, as illustrated in [figure 7](#), the diode D becomes forward-biased. Inductor LA transfers energy to the coupling capacitor Cc, while inductor LB supplies energy to the output, maintaining the necessary power for the load. This switching cycle allows the SEPIC converter to regulate the output voltage effectively across varying input conditions.

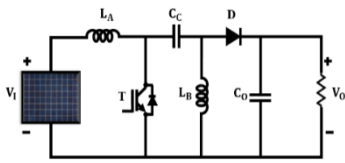


Figure 5. SEPIC converter

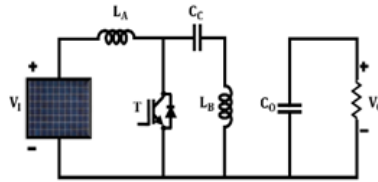


Figure 6. T ON condition

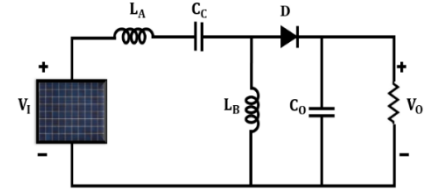


Figure 7. T OFF condition

The duty cycle of the SEPIC converter can be expressed by the following equation:

$$D = \frac{V_O + V_D}{V_i + V_O + V_D} \quad (1)$$

This equation indicates that the duty ratio is influenced by both the output voltage (V_O) and the voltage drop across the diode (V_D), in relation to the input voltage (V_i) and output. The inductance values for both inductors L_A and L_B are derived from the minimum input voltage, ripple current, and switching frequency, as follows:

$$L_A = L_B = \frac{V_{i(\min)}}{\Delta I_L * f_{sw}} \quad (2)$$

Here, ΔI_L represents the ripple current in the inductors, which is typically around 40% of the output current, given by:

$$I_o * \frac{v_o}{V_{i(\min)}} * 40\% \quad (3)$$

The switching frequency, denoted as f_{sw} , also plays a critical role in determining the inductance values. Additionally, the peak voltage across the MOSFET is defined by the sum of the input and output voltages, as represented by:

$$VP = V_i + V_o \quad (4)$$

Similarly, the peak current through the MOSFET, which is the sum of the peak currents of inductors L_A and L_B , is given by:

$$P=ILAP+ILBP \quad (4)$$

The minimum peak reverse voltage of the diode is determined by the maximum values of the input and output voltages:

$$VPRD = V_i (\max) + V_o (\max) \quad (5)$$

To calculate the RMS current through the coupling capacitor, the following equation is used, which takes into account the output current and the ratio of the output voltage to the minimum input voltage:

$$I_c(\text{rms}) = I_o * \sqrt{\frac{V_o + V_D}{V_{i(\min)}}} \quad (6)$$

Lastly, the output capacitor's RMS current can be determined by the following equation, which relates the output current, duty cycle, voltage ripple, and switching frequency:

$$C_o \geq \frac{I_o * D}{V_{rip} * 0.5 * f_{sw}} \quad (7)$$

In comparison to other traditional converters, the SEPIC converter offers a higher voltage gain and output power. This gain is directly proportional to the duty cycle, meaning that as the duty ratio increases, so does the voltage gain, making the SEPIC converter a more efficient option for certain applications.

3.6. Switching operation of SEPIC by CNN and SOC estimation

Neural networks and other machine learning techniques have demonstrated potential for estimating SOC because of their capacity to extract intricate correlations from data. When CNN-based control as depicted in figure 8 is used in SEPIC converters and battery management system, the neural network is usually trained using experimental or simulation data in order to determine the best control strategy. SEPIC converters can achieve more efficiency, increased dependability, and improved performance in solar power conversion applications by utilizing sophisticated control techniques including CNN-based control and SOC estimates. This will ultimately help to progress sustainable energy systems.

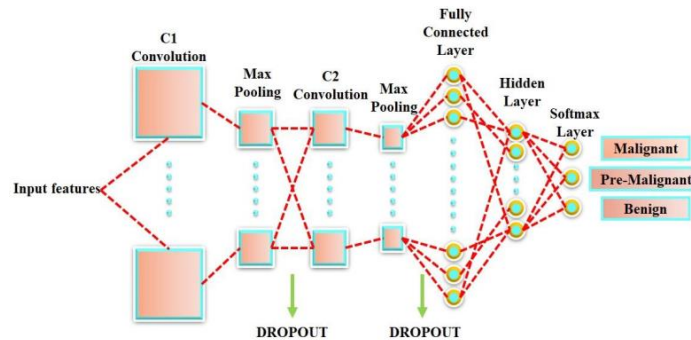


Figure 8. CNN structure

Voltage, current, temperature, and maybe other environmental or system factors are among the input-output data from the battery system that SOC estimate algorithms commonly used to train the estimation model. Here, the concern voltage attained after the SEPIC equipment diverges at every instant and doesn't remain firm owing to interpretations in the cosmological intensity and hotness. From now on, a CNN regulator oversees controlling the helicopter's switching maneuver in order to make the affair even more firm and careful by reducing ripple content. The factual voltage V_{act} attained from the chopper is coordinated with the mentioned voltage V_{ref} , and an inaccuracy is engendered. This inaccuracy is furnished as a contribution to the CNN regulator, a governor gesture is generated that's fed to the pulse width modulation generator. The pulse width modulation generator originator produces a triggering signal, which governs the switching maneuver of the chopper for a meticulous affair with no deformation.

To prevent the battery from charging or draining, the SOC is continuously covered in verification. Using the CNN controller shortens the charging time and extends the battery life. When the battery's SOC falls below the prescribed value, the charging process initiates, and when the SOC rises above the set value, the CNN controller initiates the discharging task.

4. Results and Discussion

Figure 9 shows the MATLAB Simulink view. The CNN predicated SOC witnessing strategy is the substantial nexus of anticipated investigation work. In addition to witnessing SOC, CNN is also employed for the governor of non-isolated chopper. The functional interpretation of the propounded approach is analyzed using MATLAB replication. The constraints for the photovoltaic cell and the non-isolated SEPIC chopper are given in table 1.

Table 1. Photovoltaic cell and non-isolated SEPIC

Parameter	Values
	<i>Solar Panel</i>
Power	2000 W
Required panels	100 W, 20 panels

V_{SC}	12 V
V_{OC}	22.6 V
I_{SC}	8.33 A

SEPIC converter

Inductors (L_1, L_2)	1mH
Capacitors (C_1, C_2)	22 μ F
Switching Frequency	10kHz

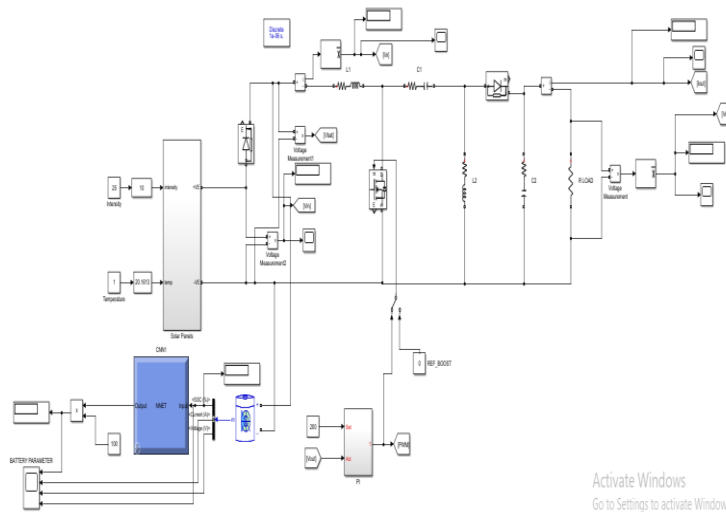


Figure 9. MATLAB Simulink view

The PV panel voltage waveform, shown in figure 10(a), depicts a steady DC voltage. In general, it stays constant while there is enough solar radiation present. The voltage is 28 volts. The PV panel current waveform, shown in figure 10 (b), is 10-50A. Figure 10(a) shows the transfiguration of photovoltaic output to an imperative position is prosecuted employing a non-isolated SEPIC chopper, which is an altitudinous accretion chopper, by means of a reversed signal in extension to minimal losses.

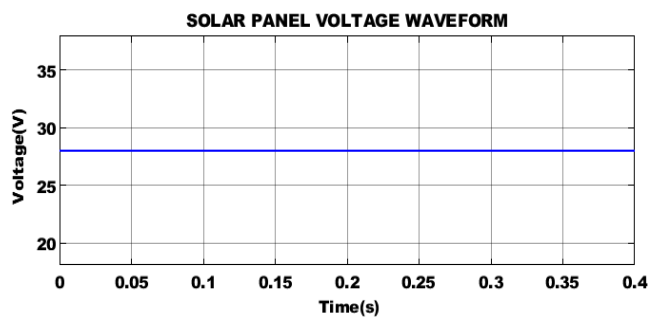


Figure 10a. PV voltage waveform

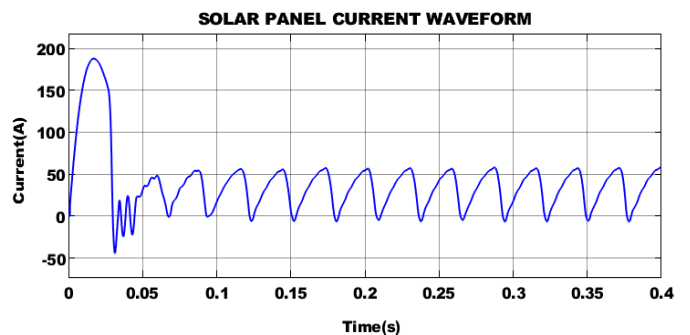


Figure 10b. PV current waveform

The non-isolated SEPIC chopper delivers a voltage of 190V and a current of 3.88A, as specified in figure 11(a) and figure 11(b). The practice of the CNN is handled by means of experimental statistics that are acquired by the sequence and are suited offline and exclusively when linkage diverges to an inferior loss inception and linkages are pertained online. During an online mission, a frontward permit is claimed in distribution to evaluate the SOC. Backward passes are no longer challenged once the miniature is properly conditioned.

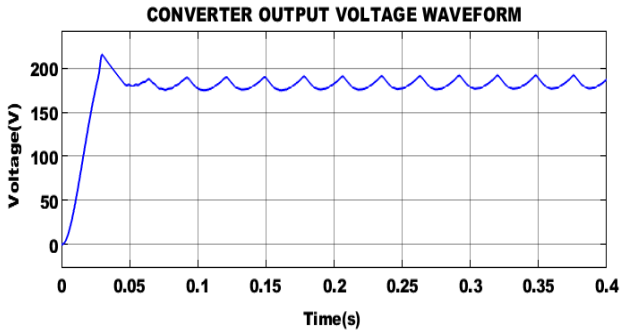


Figure 11a. Output voltage of non-isolated chopper

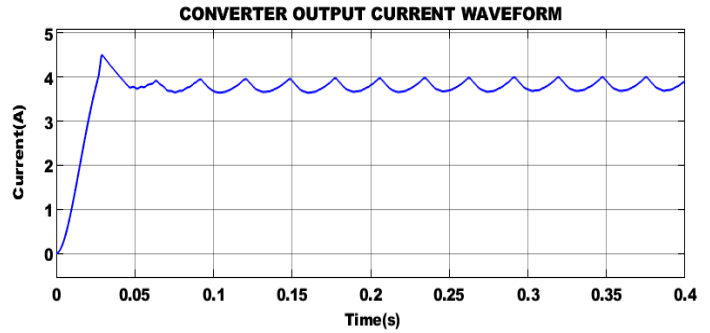


Figure 11b. Output current of non-isolated chopper

CNNs offer a high ground of fast computing time, as was previously conditioned since a forward pass is mostly made up of a series of matrix expansions. The practice of CNN is handled by means of experiment statistics that are acquired through the sequence and are suited to offline mode, and exclusively when mesh meets a minor loss verge can the meshes be pertained online. Throughout the online maneuver, exclusively a forward pass is demanded in sequence to evaluate SOC. Backward passes are no longer needed once the prototypical is properly accomplished. CNNs offer the benefit of faster calculation time, which was already fully developed, and then a forward pass is made up of a lot of matrix proliferations. The confirmation progression of merging the CNN by means of a contemporary test bench is substantially covered by the structure of matrix proliferations. Predicated on the 2-concealed subcaste arrangement of the machine literacy prototypical, three weight- and three bias-arrangements that traits to this prototypical are uprooted, for instance, six CSV lines and protected into Beagle Bone Black for SOC computation. The sequencer that plans the addition of matrices is inscribed in Python, The NumPy platform delivers the competency of recycling huge quantities of statistics in a fast-moving mode. The workout time diverges according to the quantity of bumps at each level.

The computing time varies according to the number of nodes in each layer. For instance, a model that contains 4000 nodes on each hidden layer often takes 10 minutes for one-time SOC calculation; whereas 8 minutes is needed for a model with 2400 nodes in each layer, a 300- node model only demands 90 second. However, the more nodes in each layer contributes to a more accurate SOC result. The mean-absolute errors of the models from all test data are 1.12%, 1.13% and 3.27%, independently. The further bumps in respective levels contribute to a more exact SOC outcome. The mean-absolute crimes of the forenamed representations after all investigation information are shown [figure 12\(b\)](#). For these explanations, a skill is tainted between calculation period and delicacy. In this exploration, the quantity of bumps in each retired level for charge is preferred to be 2400; subsequently, it realizes an accurate outcome, whereas possession requires sensible calculation time. The scope of CNN for discharge is named to be 2500 bumps on each retired level; this one can achieve 0.80 MAE.

The [figure 12\(a\)](#) and [figure 12\(b\)](#) signifies the position of the current (1A) and voltage (24V) outputs in the battery. The engendered power from the Photo Voltaic is stowed in the battery. Throughout the attainability of the principal cause of power force, the battery, which acts as a subordinate control cause, releases, and handovers control to the cargo.

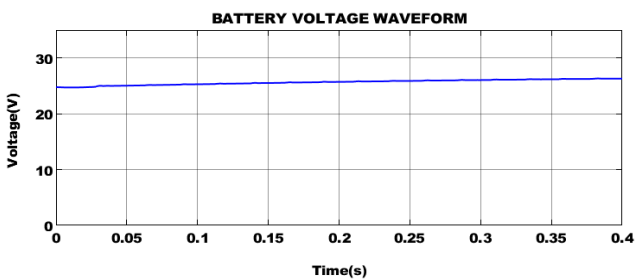


Figure 12a. Battery Current waveform

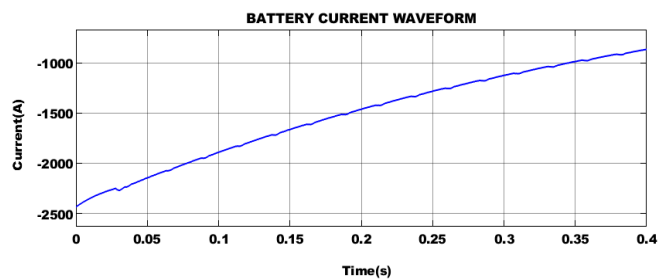


Figure 12b. Battery voltage waveform

The state of charge of the battery is 94 from experimental validation, as illustrated in [figure 13](#) CNN does a great job at examining the battery's state of charge. The confirmation procedure for merging the CNN through a contemporary

test bench encompasses substantially the structure of matrix proliferations. Following the two-hidden subcaste arrangement of the machine literacy prototypical, three weight- and three bias-arrays that are similar to this prototypical are taken out, for example six CSV lines, and saved in Beagle Bone Black for SOC computation. The sequencer that performs the addition of matrices is inscribed in MATLAB, which delivers the competence of recycling huge quantities of data in a speedy manner.

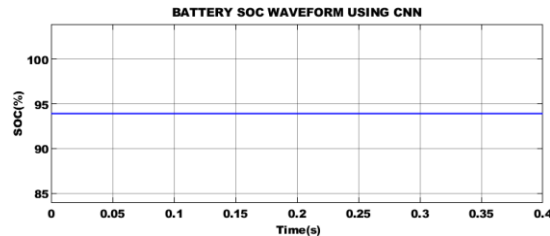


Figure 13. SOC of Battery

The figure 14 shows the Hardware implementation of CNN for battery system monitoring and predicted SOC for Electric Vehicle. In contrast to conventional methods of estimating SOC, the CNN-SOC model can compensate for estimation deviations resulting from voltage jumps at the end of charge and discharge. It can also yield satisfactory SOC estimation results during the stabilized stage and during different phases of charging and discharging the system's assembled batteries. The outcomes show that this approach allows for quick and precise SOC estimation

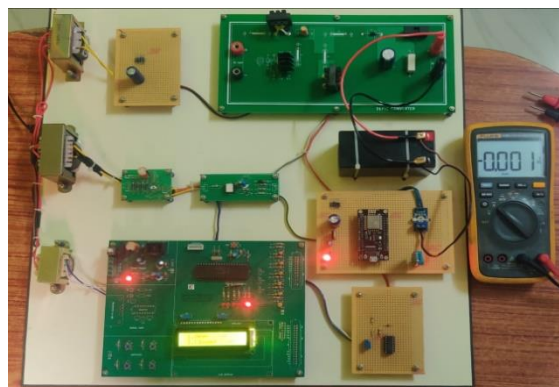


Figure 14. Battery SOC System Hardware view

5. Conclusion

The CNN-predicted SOC coverage mechanism is the main subject of this work. The constant need for electricity, in addition to concerns about the quantity and rate of residual energies, has pushed the installation of massive clean power generation systems in recent years. To achieve effective energy conversion, SEPIC is used as a bidirectional converter with a high voltage gain. The work conveys the input as photovoltaic energy and the battery's SOC, which is managed by the CNN to maintain the charging and discharging processes. The SoC and error estimation are obtained from the CNN of the battery. Also, the work links to the operation of the proposed system

Over the next five years, the battery management system is projected to rise five to seven times. According to optimistic estimates, it will reach about 35 billion dollars by 2026 from its 2020 valuation of 5 billion dollars, meaning that within five years, electric vehicles will account for 15% of all automotive sales globally. If we look ahead 73 years, we will witness significant advancements in the state of charging technology. It will resemble the process of refueling, for example. The voltage at which cars may be charged will rise from 500V to 800V in the upcoming years. Additionally, the capacity of a single charger will increase to 350 kW from its current 60 kW. This means that the charging time will be reduced from around one hour.

The experience of charging an EV would undergo a change thanks to IoT. To maximize resource utilization and improve the charging experience, it will intelligently connect grids, networks, renewable energy sources, batteries, and automobiles. The Internet of Vehicles, or IoV, would be the name of this system. Electric buses and trucks will become

much more in demand. Prominent corporations such as Amazon and Walmart aspire to project an image of environmental sustainability. Their present plan includes using commercial vehicles with zero emissions. Because of this, companies involved in EV charging would have to build mega-chargers to enable these massive electric cars to be driven over great distances.

The planned apparatus was tested on a laboratory scale and can be installed in mine substations under the right safety measures to ensure that it functions as intended in an actual mining environment. While using automatic PF correction, a harmonic problem may arise from the repeated switching of the capacitor bank while the load is changing regularly. To prevent frequent switching of the capacitor bank, an appropriate filter design and an optimal algorithm design can be carried out based on the pattern of frequent load changes. To determine the best position for maximum utilization and cost savings, comparative research on the placement of correctional equipment may be used in the field. This is also an option for several applications that focus on improving efficiency [13].

6. Declarations

7.1. Author Contributions

Conceptualization: P.S., V.K.P., S.V., M.B., and G.D.; Methodology: S.V. and M.B.; Software: P.S.; Validation: P.S., V.K.P., and M.B.; Formal Analysis: P.S. and V.K.P.; Investigation: S.V. and G.D.; Resources: M.B.; Data Curation: V.K.P.; Writing Original Draft Preparation: P.S., V.K.P., and S.V.; Writing Review and Editing: M.B. and P.S.; Visualization: V.K.P.; All authors have read and agreed to the published version of the manuscript.

7.2. Data Availability Statement

The data presented in this study are available on request from the corresponding author.

7.3. Funding

The authors received no financial support for the research, authorship, and/or publication of this article.

7.4. Institutional Review Board Statement

Not applicable.

7.5. Informed Consent Statement

Not applicable.

7.6. Declaration of Competing Interest

The authors declare that they have no known competing financial interests or personal relationships that could have appeared to influence the work reported in this paper.

References

- [1] T. Thangam, K. Muthuvel, and K. Eswaramoorthy, "SEPIC converter with closed loop PI controller for grid utilized PV system," *Journal of Next Generation Technology (JNxtGenTech)*, vol. 1, no. 1, pp. 1-10, 2021.
- [2] M. E. Kabir, C. Assi, H. Alameddine, J. Antoun, and J. Yan, "Demand-aware provisioning of electric vehicles fast charging infrastructure," *IEEE Transactions on Vehicular Technology*, vol. 69, no. 7, pp. 6952-6963, Jul. 2020.
- [3] J. Ruan and Q. Song, "A novel dual-motor two-speed direct drive battery electric vehicle drivetrain," *IEEE Access*, vol. 7, no. 1, pp. 54330-54342, 2019.
- [4] H. N. de Melo, J. P. F. Trovão, P. G. Pereirinha, H. M. Jorge, and C. H. Antunes, "A controllable bidirectional battery charger for electric vehicles with vehicle-to-grid capability," *IEEE Transactions on Vehicular Technology*, vol. 67, no. 1, pp. 114-123, Jan. 2018.
- [5] D. Said and T. Mouftah, "A novel electric vehicles charging/discharging management protocol based on queuing model," *IEEE Transactions on Intelligent Vehicles*, vol. 5, no. 1, pp. 100-111, Mar. 2020.
- [6] B. Wang, P. Dehghanian, S. Wang, and M. Mitolo, "Electrical safety considerations in large-scale electric vehicle charging stations," *IEEE Transactions on Industry Applications*, vol. 55, no. 6, pp. 6603-6611, Dec. 2019.

-
- [7] X. Hu, H. Wang, and X. Tang, "Cyber-physical control for energy-saving vehicle following with connectivity," *IEEE Transactions on Industrial Electronics*, vol. 64, no. 11, pp. 1-10, Nov. 2017.
- [8] B. Liu, L. Wang, D. Song, M. Su, J. Yang, D. He, Z. Chen, and S. Song, "Input current ripple and grid current harmonics restraint approach for single-phase inverter under battery input condition in residential photovoltaic/battery systems," *IEEE Transactions on Sustainable Energy*, vol. 9, no. 4, pp. 1957-1968, Oct. 2018.
- [9] M. F. Alsharekh, S. Habib, D. Dewi, A. Albattah, M. Islam, and S. Albahli, "Improving the efficiency of multistep short-term electricity load forecasting via R-CNN with ML-LSTM," *Sensors*, vol. 22, no. 18, pp. 6913-6925, Sep. 2022.
- [10] M. Mostafa, M. Mahfouz, and R. Iravani, "Grid-integration of battery-enabled DC fast charging station for electric vehicles," *IEEE Transactions on Energy Conversion*, vol. 35, no. 1, pp. 375-385, Mar. 2020.
- [11] N. Saxena, I. Hussain, B. Singh, and A. L. Vyas, "Implementation of a grid-integrated PV-battery system for residential and electrical vehicle applications," *IEEE Transactions on Industrial Electronics*, vol. 65, no. 8, pp. 6592-6601, Aug. 2018.
- [12] R. Khezri, A. Mahmoudi, and M. H. Haque, "Optimal capacity of solar PV and battery storage for Australian grid-connected households," *IEEE Transactions on Industry Applications*, vol. 56, no. 5, pp. 5319-5329, Sep. 2020.
- [13] V. M. Iyer, S. Gulur, G. Gohil, and S. Bhattacharya, "An approach towards extreme fast charging station power delivery for electric vehicles with partial power processing," *IEEE Transactions on Industrial Electronics*, vol. 67, no. 10, pp. 8076-8087, Oct. 2020.
- [14] S. F. Pratama and D. Sugianto, "Temporal Patterns in User Conversions: Investigating the Impact of Ad Scheduling in Digital Marketing," *J. Digit. Mark. Digit. Curr.*, vol. 1, no. 2, pp. 165-182, 2024
- [15] A. R. Yadulla, M. H. Maturi, K. Meduri, G. S. Nadella, "Sales Trends and Price Determinants in the Virtual Property Market: Insights from Blockchain-Based Platforms," *Int. J. Res. Metav.*, vol. 1, no. 2, pp. 113-126, 2024
- [16] S. Modi, J. Bhattacharya, and P. Basak, "Convolutional neural network-bagged decision tree: A hybrid approach to reduce electric vehicle's driver's range anxiety by estimating energy consumption in real-time," *Soft Computing*, vol. 25, no. 2, pp. 2399-2416, 2020.
- [17] Z. Zhang, L. Lu, Y. Li, H. Wang, and M. Ouyang, "Accurate remaining available energy estimation of LiFePO₄ battery in dynamic frequency regulation for EVs with thermal-electric-hysteresis model," *Energies*, vol. 2023, no. 1, pp. 1-10, Jan. 2023.
- [18] B. H. Hayadi and I. M. M. El Emary, "Enhancing Security and Efficiency in Decentralized Smart Applications through Blockchain Machine Learning Integration", *J. Curr. Res. Blockchain.*, vol. 1, no. 2, pp. 139-154, Sep. 2024.
- [19] Z. Zhang, X. Cheng, Z.-Y. Lu, and D.-J. Gu, "SOC estimation of lithium-ion batteries with AEKF and wavelet transform matrix," *IEEE Transactions on Power Electronics*, vol. 32, no. 10, pp. 7626-7634, Oct. 2017.
- [20] Y. Wang, C. Zhang, and Z. Chen, "On-line battery state-of-charge estimation based on an integrated estimator," *Applied Energy*, vol. 185, no. 1, pp. 2026-2032, Jan. 2017.